Universiteit Leiden
The Netherlands

(Automated) synthesis of well-defined staphylococcus aureus wall teichoic acid fragments

Ali, S.; Hendriks, A.; Dalen, R. van; Bruyning, T.; Meeuwenoord, N.; Overkleeft, H.S.; ... ; Codee, J.D.C.

(Automated) Synthesis of Well-defined *Staphylococcus Aureus* Wall Teichoic Acid Fragments

Sara Ali,[a] Astrid Hendriks,[b] Rob van Dalen,[b] Thomas Bruyning,[a] Nico Meeuwenoord,[a] Herman S. Overkleeft,[a] Dmitri V. Filippov,[a] Gijs A. van der Marel,[a] Nina M. van Sorge,[b] and Jeroen D. C. Codée*[a]

Abstract: Wall teichoic acids (WTAs) are important components of the cell wall of the opportunistic Gram-positive bacterium *Staphylococcus aureus*. WTAs are composed of repeating ribitol phosphate (RboP) residues that are decorated with D-alanine and *N*-acetyl-D-glucosamine (GlcNAc) modifications, in a seemingly random manner. These WTA-modifications play an important role in shaping the interactions of WTA with the host immune system. Due to the structural heterogeneity of WTAs, it is impossible to isolate pure and well-defined WTA molecules from bacterial sources. Therefore, here synthetic chemistry to assemble a broad library of WTA-fragments, incorporating all possible glycosylation modifications (α-GlcNAc at the RboP C4; β-GlcNAc at the RboP C4; β-GlcNAc at the RboP C3) described for *S. aureus* WTAs, is reported. DNA-type chemistry, employing ribitol phosphoramidite building blocks, protected with a dimethoxy trityl group, was used to efficiently generate a library of WTA-hexamers. Automated solid phase syntheses were used to assemble a WTA-dodecamer and glycosylated WTA-hexamer. The synthetic fragments have been fully characterized and diagnostic signals were identified to discriminate the different glycosylation patterns. The different glycosylated WTA-fragments were used to probe binding of monoclonal antibodies using WTA-functionalized magnetic beads, revealing the binding specificity of these WTA-specific antibodies and the importance of the specific location of the GlcNAc modifications on the WTA-chains.

Introduction

The Gram-positive bacterium *Staphylococcus aureus (S. aureus)* is a common member of the human microbiome and is commonly found on the skin and in the nares. When entering the blood stream or internal tissues, *S. aureus* can cause serious infections, for which immunocompromised patients are especially at risk.[1] Extensive use of antibiotics has resulted in increased resistance among *S. aureus* strains against commonly-used antibiotics leading to infections that are difficult to treat. Currently, methicillin -resistant *S. aureus* (MRSA) is the most commonly identified antibiotic-resistant pathogen in clinical medicine worldwide.[2] The spread of MRSA highlights the

urgent need for alternative therapies, such as passive or active vaccination.[3] Wall teichoic acids (WTAs) are prime constituents of the Gram-positive cell wall and can function as effective antigenic epitopes. WTAs are therefore promising candidates for the development of a conjugate vaccine against *S. aureus* infections.[4] WTAs are anionic poly(ribitol phosphate) (RboP) chains covalently attached to the thick peptidoglycan layer of the bacterial cell wall. They are involved in a plethora of vital bacterial functions including host interaction, biofilm formation, autolysin activity and their overexpression can increase bacterial virulence.[5] The ribitol residues that are interconnected through phosphodiester linkages, can be substituted in a seemingly random manner with D-alanine (D-Ala) on C2, α/β-*N*-acetyl-D-glucosamine (GlcNAc) on C-4 or a β-GlcNAc on C-3. The GlcNAc residues are introduced by three dedicated glycosyltransferases, TarS[6] (1,4-β-GlcNAc), TarM[7] (1,4-α-GlcNAc), and the recently discovered TarP[8] (1,3-β-GlcNAc), respectively (See Figure 1).

To unravel the roles of WTAs in biology at the molecular level, well-defined fragments are indispensable tools. Since isolation from the bacteria leads to heterogenous mixtures of fragments and bacterial contaminations, organic synthesis is the method of choice to generate WTA-fragments with pre-defined substitution pattern. Because the WTA fragments are built up from repeating units interconnected through phosphodiester linkages, well-established DNA chemistry can be used to assemble the target compounds, also offering the possibility for automation. Over the years, several approaches have been reported for the assembly of both WTAs as well as the structurally-related lipoteichoic acids (LTAs). We have reported

[a] S. Ali, T. Bruyning, N. Meeuwenoord, Prof. Dr. H. S. Overkleeft,
     Dr. D. V. Filippov, Prof. Dr. G. A. van der Marel, Prof. Dr. J. D. C. Codée
     Leiden Institute of Chemistry
     Leiden University
     Einsteinweg 55, 2333 CC Leiden (The Netherlands)
     E-mail: jcodee@chem.leidenuniv.nl

[b] A. Hendriks, R. van Dalen, Dr. N. M. van Sorge
     Medical Microbiology, University Medical Center Utrecht
     Utrecht University
     Heidelberglaan 100, 3584 CX Utrecht (The Netherlands)

Chemistry–A European Journal

Full Paper
doi.org/10.1002/chem.202101242

Chemistry
Europe
European Chemical
Societies Publishing
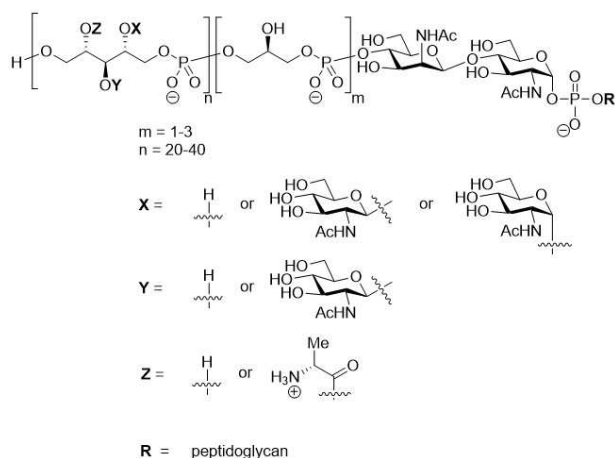
Figure 1. Schematic representation of *S. aureus* WTA structure.

techniques. All fragments are equipped with an aminohexanol spacer for conjugation purposes. Taking into account that bacterial WTA is covalently attached to peptidoglycan at the RboP C1-position, this is also the attachment site for the linker in the synthetic fragments. We have equipped the synthetic fragments with a biotin handle, and we have used these to functionalize streptavidin coated, magnetic beads to generate WTA beads that have been used to characterize the binding of several monoclonal antibodies at the molecular level.[12] These binding studies have cleanly revealed the binding specificity and differences between these antibodies, not only showing clear differences between monoclonal antibodies recognizing the α- or β-linked GlcNAc ribitolphosphates, but also selectivity between the regioisomeric β-GlcNAc WTA fragments. The synthetic WTA oligomers thus represent valuable tools in mapping binding specificity of host receptor molecules at the molecular level.

on different strategies to assemble glycerol phosphate-based LTA fragments, including solution phase, fluorous-tag based and automated solid phase syntheses.[9] The synthesis of RboP WTA fragments has been described before by the groups of Pozsgay,[10] Lee,[11] and Driguez,[4b] each building on the use of phosphoramidite chemistry. Pozsgay and Lee however reported that automation of their syntheses was unsuccessful. We here report on the development of chemistry that allows for the generation of well-defined unsubstituted RboP oligomers, using both solution and automated solid phase synthesis (ASPS)

Results and Discussion

The set of compounds, generated for this study is depicted in Figure 2. All fragments are functionalized with an aminohexanol spacer for conjugation purposes. We have previously described that a glycosylated glycerol phosphate hexamer LTA fragment can be used as an adequate synthetic antigen in the development of vaccines against *Enterococcus faecalis*.[13] We therefore decided to target a set of glycosylated ribitol phosphate WTA hexamers. In addition, we aimed to assemble longer non-
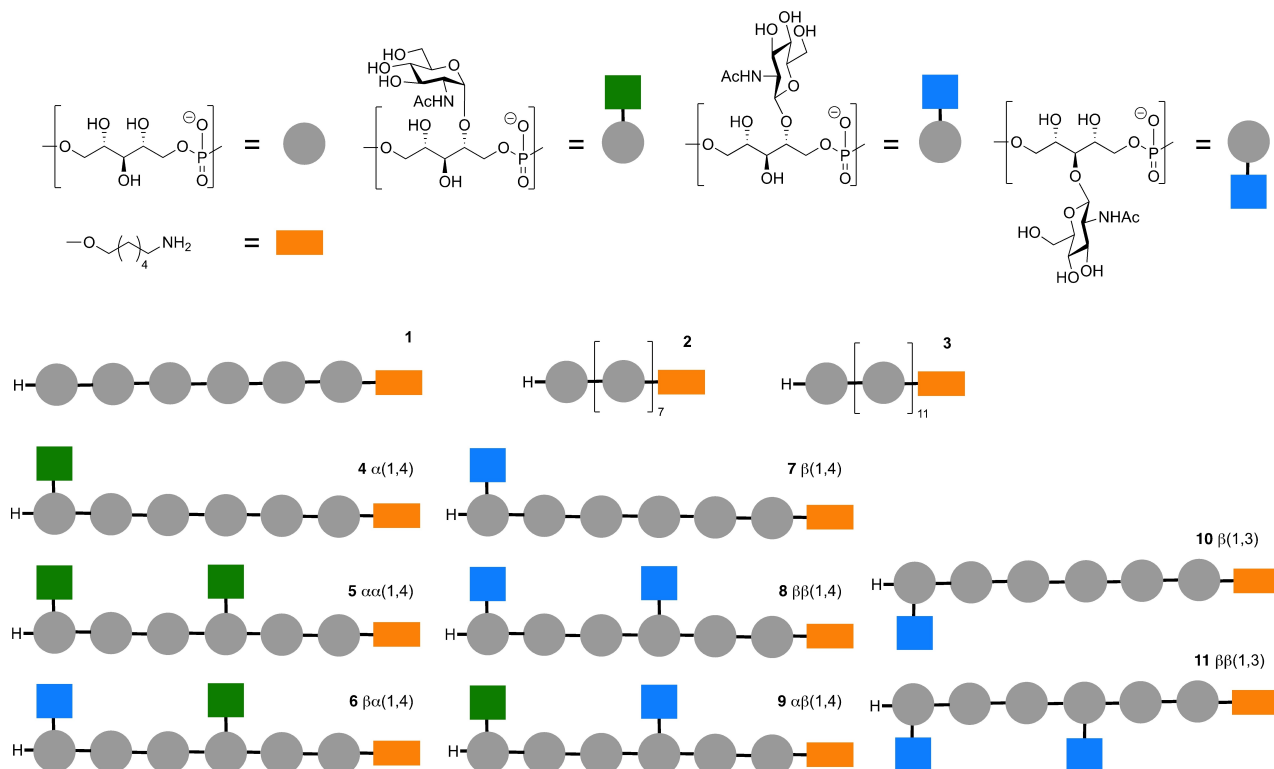

Figure 2. The library of RboP-WTA structures, generated for this study.

Chemistry–A European Journal

Full Paper
doi.org/10.1002/chem.202101242

Chemistry
Europe
European Chemical
Societies Publishing

substituted fragments through automated synthesis. The set thus comprises RboP-WTA chains carrying no carbohydrate substituents varying in length from a hexamer (**1**) to an octamer (**2**) and a dodecamer (**3**). Different carbohydrate decoration patterns have been introduced (α-GlcNAc or β-GlcNAc residues can be mounted on the C4-hydroxy groups of the RboP-monomers or the RboP C3-hydroxy can carry a β-GlcNAc) and we decided to mount a single GlcNAc residue at the terminal RboP residue, or two GlcNAc residues at the third and the sixth RboP. Besides the hexamers carrying a single type of carbohydrate appendage, we also generated two hexamers having both an α-(1,4)-GlcNAc and a β-(1,4)-GlcNAc on the RboP-chain, leading to the following set of target compounds: α(1,4) **4**, and αα(1,4) **5**, βα(1,4) **6**, β(1,4) **7**, ββ(1,4) **8**, αβ(1,4) **9**, β(1,3) **10** and ββ(1,3) **11**.

Synthesis of building blocks

The building blocks that we designed for the assembly of the target compounds are depicted in Scheme 1A. The ribitol phosphate building blocks feature a temporary dimethoxytrityl group to mask the primary alcohol that is to be elongated during the chain elongation and a cyanoethyl phosphoramidite functionality. Ribitol building blocks **13**, **14** and **15** carry an α-(1,4), β-(1,4) and β-(1,3)-linked N-acetyl glucosamine appendage, respectively, and the carbohydrate moieties in these building blocks only carry benzyl ether protecting groups to allow for the global deprotection of the fragments using mild hydrogenation conditions. We used phosphoramidite hexanol-amine **16**[9a] to introduce the amino linker in the molecules.

The synthesis of ribitol phosphoramidite **12** was accomplished as described by Hermans et al.[14] Scheme 1B depicts the synthesis of the glycosylated building blocks **13**, **14** and **15**. The synthesis of the required C4-OH ribitol **20**, started from ribose **17** by allylation of the primary alcohol, followed by isopropylidene hydrolysis to yield **18**. Benzylation and ensuing acidic hydrolysis of the methyl acetal yielded the corresponding lactol intermediate, which was reduced using sodium borohydride to provide primary alcohol **19**. Protection with a TBDPS group then gave acceptor **20**. Driguez and Lee previously described the use of a glycosylation strategy in which a mixture of α- and β-N-acetyl glucosamine was generated. We set out to develop stereoselective glycosylation methodology to streamline the assembly of the glycosylated building blocks.

The assembly of the α-linked GlcNAc building block was accomplished using glucosazide donor **21**, which was coupled with acceptor **20** to yield **22** as a 7:1 α/β-mixture. The two anomers could be separated after Zemplén deacetylation, leading to the pure α-product **23** in 70% yield.[15] Benzylation of the liberated alcohols, followed by Staudinger reduction and subsequent acetylation of the amine yielded **24** in 89% yield over 3 steps. Next the TBDPS group was exchanged for a 4,4′-Dimethoxytrityl (DMTr) group to afford **25**. The removal of the allyl ether was accomplished by the iridium catalyzed allyl isomerization and iodine mediated enol ether hydrolysis, under slightly basic conditions to deliver alcohol **26**, which was

functionalized with a cyanoethyl phosphoramidite to give the building block **13** in 81% yield.

The corresponding β-GlcNAc building block was generated through the union of tribenzyl glucosazide donor **27** and acceptor **20**. The use of acetonitrile as a β-directing solvent in combination with a low reaction temperature ensured the stereoselective formation of the desired β-glucosamine linkage and **28** was obtained in 85%.[16] Similar protecting group manipulations as described for the α-GlcNAc ribitol then delivered the required β-GlcNAc building block **14**.

The synthesis of the β-(1,3)-GlcNAc-functionalized ribitol phosphoramidite **15** required the generation of C3-OH ribitol **40**.
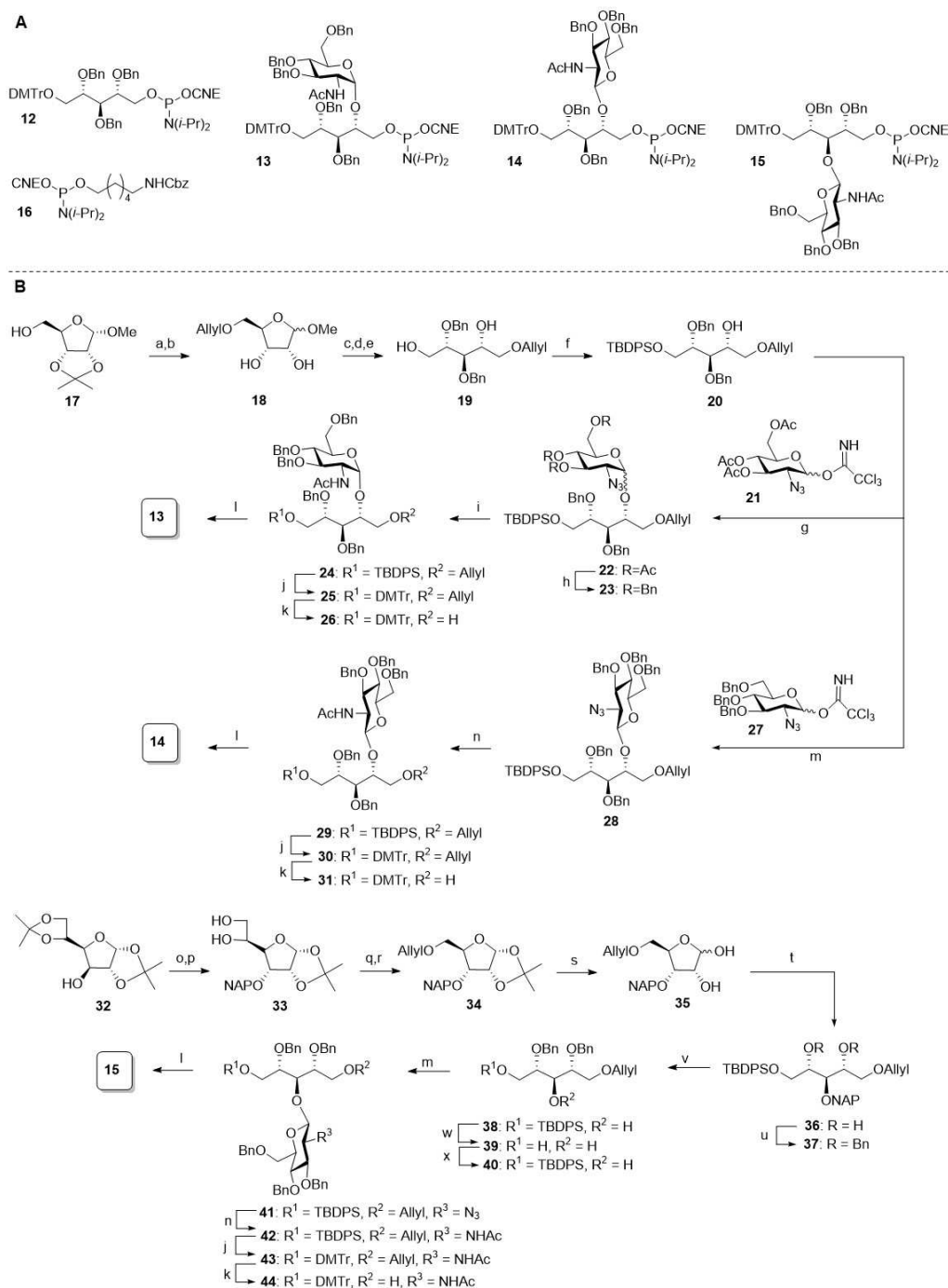
To this end, diacetone-D-glucose **32** was transformed into the corresponding allose, having the required ribose stereochemistry, through a well-established[17] oxidation-reduction sequence in 69% yield. Naphthylation then gave the fully protected allofuranose and regioselective removal of the 5,6-isopropylidene group using p-TsOH in MeOH provided compound **33** in 75% over 2 steps. Next, oxidative cleavage of the 5,6-diol with $NaIO_4$ gave the aldehyde, which was reduced to form the primary alcohol. Allylation of this alcohol, afforded ribose **34** with a yield of 88% over 3 steps. Subsequently, the 1,2-isopropylidene was cleaved under acidic conditions to give **35**. Reductive opening of hemiacetal **35**, and TBDPS protection of the primary alcohol then provided **36**. Benzylation of the remaining alcohols led to fully protected ribitol **37**. During this alkylation step, a byproduct formed, due to TBDPS migration and this product could not be separated from the desired product at this stage. Therefore, the naphthyl ether and TBDPS ethers were removed to provide **38**, which could be purified from the formed byproduct yielding product **39** in 62% yield over 3 steps. Reinstallation of the TBDPS group on the primary alcohol furnished the C3-OH ribitol building block **40**.

The glycosylation of **40** was accomplished using donor **27** and the reaction conditions described above delivered the glucosamine ribitol **41** as a single anomer in 80% yield. This synthon was uneventfully transformed into the desired β-(1,3)-GlcNAc ribitol phosphoramidite **15** using the protecting and functional group manipulations described above.

Assembly of RboP WTA fragments
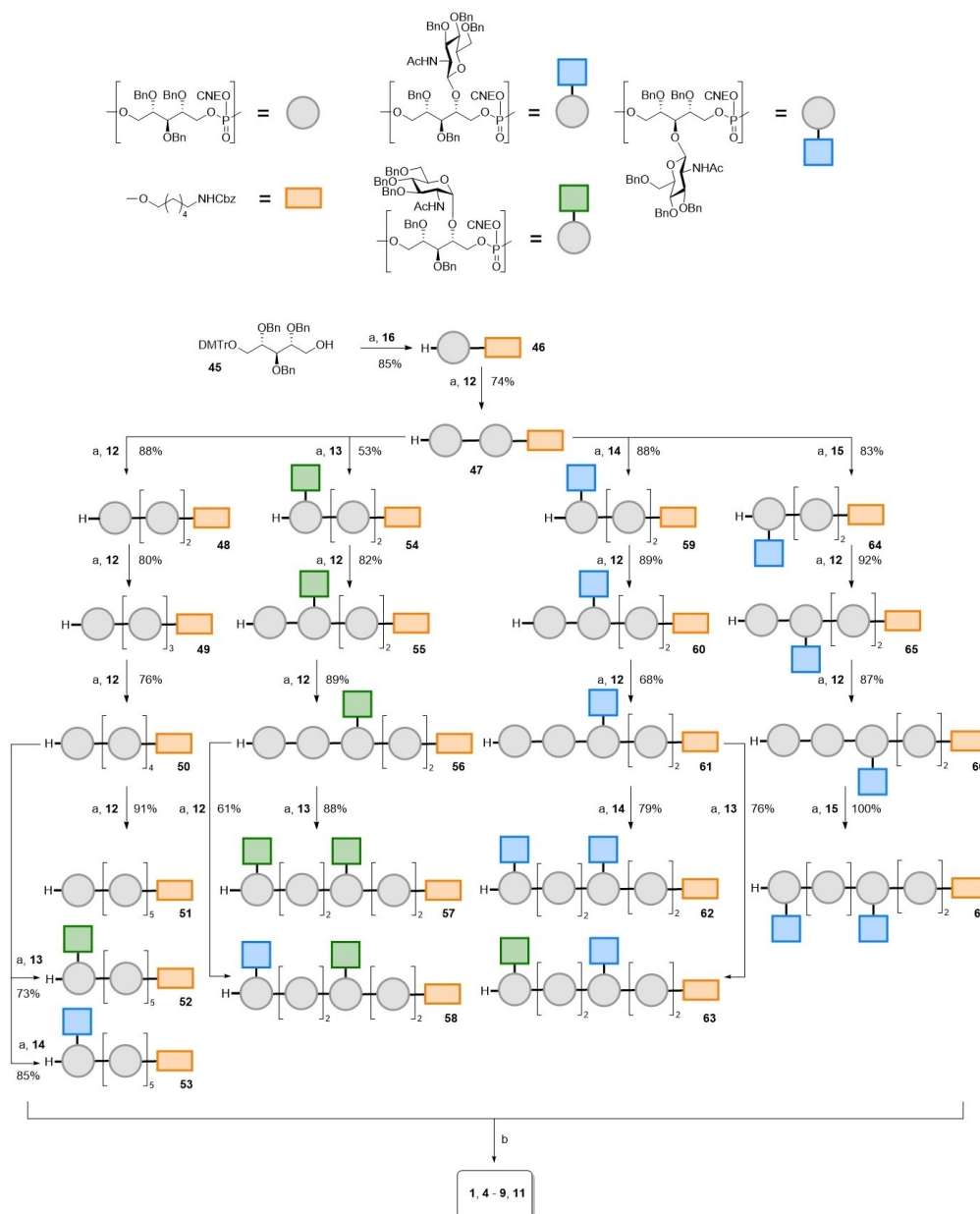
Solution phase synthesis of RboP WTA fragments

With all required building blocks in hand, we set out to generate the set of target structures, using a solution phase synthesis approach depicted in Scheme 2. First the coupling chemistry was explored in the synthesis of non-substituted hexamer **1**. The RboP-chain elongation steps using phosphoramidite condensations consisted of 3 steps. In the first step the amidite was activated under agency of 4,5-dicyanoimidazole (DCI) to enable attack by the primary ribitol alcohol to form the phosphite intermediate, which was oxidized in the next step using (10-camphorsulfonyl)oxaziridine (CSO). Detritylation using 3% dichloroacetic acid (DCA) in DCM liberated the primary

Chemistry–A European Journal

Full Paper
doi.org/10.1002/chem.202101242

Chemistry
Europe
European Chemical
Societies Publishing

Scheme 1. Assembly of building blocks. a) AllylBr, NaH, THF/DMF (7:1), 0 °C to rt; b) AcOH/H₂O 1:1, 50 °C, 300 mbar, 62% over 2 steps; c) BnBr, NaH, THF/DMF (7:1), 0 °C to rt; d) 4 M HCl dioxane, 80 °C; e) NaBH₄, MeOH, 0 °C, 50% over 3 steps; f) TBDPSCl, TEA, DCM 0 °C to rt, 95%. g) **21**, TMSOTf, DCM, rt, 92%, 7:1 α/β; h) i. NaOMe, MeOH, rt, 70% α-anomer; ii) BnBr, NaH, THF/DMF (7:1), 0 °C to rt, 73%; i) i. PMe₃, KOH, THF; ii. Ac₂O, pyridine, **24**: 89% over 2 steps; j) i. TBAF, THF, rt; ii) DMTrCl, TEA, DCM, **25**: 67%; **30**: 36%; **43**: 60%; k) i. Ir(COD)(Ph₂MeP)₂PF₆, H₂, THF, ii. I₂, sat. aq. NaHCO₃, THF, **26**: 88%; **31**: 79%; **44**: 94%; l) 2-cyanoethyl-N,N-diisopropylchlorophosphoramidite, DIPEA, DCM, **13**: 81%; **14**: 78%; **15**: 85%; m) **27**, TMSOTf, ACN, −40 °C to 0 °C, **28**: 85%; **41**: 80%; n) propanedithiol, pyridine, H₂O, TEA, rt; ii. Ac₂O, pyridine, **29**: 59% 2 steps; **42**: 86%; o) i. DMSO, Ac₂O; ii. NaBH₄, EtOH/H₂O, 69% over 2 steps; iii. NAPBr, NaH, TBAI, THF; p) p-TsOH·H₂O, MeOH, 75% over 2 steps; q) i. 0.2 M NaIO₄ in H₂O, ethylene glycol, MeOH; ii. NaBH₄, MeOH; r) AllylBr, NaH, THF/DMF, 88%; s) THF/H₂O/formic acid, 85%; t) i. NaBH₄, MeOH; ii. TBDPSCl, TEA, DCM, 57% over 2 steps; u) BnBr, NaH, THF/DMF; v) DDQ, DCM/H₂O; w) TBAF, THF, 62% over 2 steps; x) TBDPSCl, TEA, DCM, 98%.

alcohol and silica gel column chromatography yielded the pure ribitol phosphate fragment, ready for the next elongation step. Starting with ribitol **45**[14] and spacer amidite **16**, monomer **46**

was obtained in 85% yield. From alcohol **46** the coupling cycles were repeated five times to yield **47–51**, all in good yield. Next, we incorporated the glycosylated building blocks in the
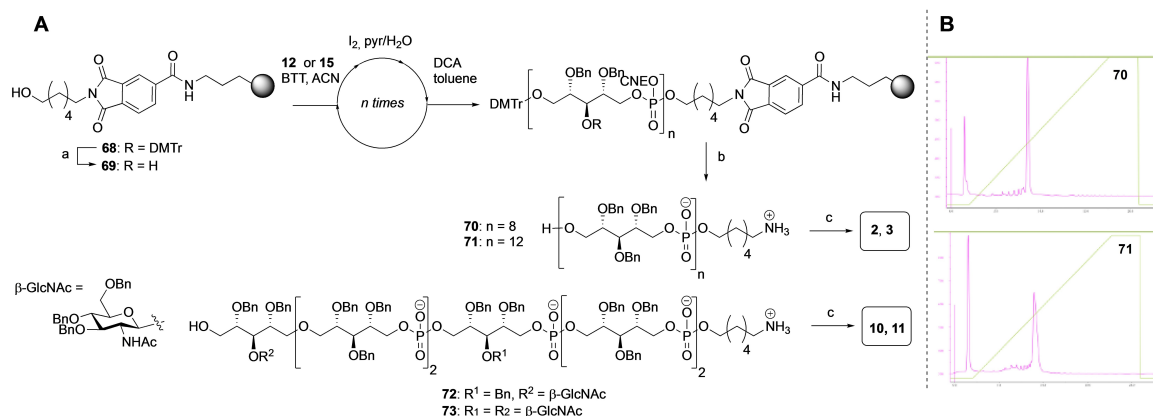
Chemistry–A European Journal

Full Paper
doi.org/10.1002/chem.202101242

Chemistry
Europe
European Chemical
Societies Publishing

Scheme 2. Assembly of the target WTA-oligomers. Reagents and conditions: a) i. DCI, ACN, phosphoramidite **12**, **13**, **14** or **15**; ii. CSO; iii. 3% DCA in DCM. b) i. NH$_3$ (30-33% aqueous solution), dioxane; ii. Pd black, H$_2$, AcOH, H$_2$O/dioxane, **1**: 87%; **4**: 96%; **5**: 55%; **6**: 16%; **7**: 68%; **8**: 78%; **9**: 88%; **11**: 70%.

synthetic scheme, generating the hexamers with one or two GlcNAc residues. All chain elongation events proceeded uneventfully and the yields for all coupling cycles are summarized in Scheme 2. The presence of the carbohydrate appendages did not seem to influence the efficiency of the condensation chemistry, reaffirming the power of phosphoramidite chemistry to assemble this type of biopolymer fragments. Deprotection of the fragments was accomplished by first removing the cyanoethyl groups to deliver the corresponding phosphate diesters followed by hydrogenation to remove all benzyl groups. All target compounds were obtained after gel permeation size exclusion purification and sodium ion exchange.

Automated solid phase synthesis of RboP WTA fragments

Finally, we investigated the possibility to assemble RboP-WTA oligomers using an automated solid phase approach (Scheme 3). To this end, we selected the commercially-available controlled pore glass (CPG) resin **68** that carries a phthalimide protected aminohexanol spacer. Previously, Pozsgay and coworkers described that an intractable mixture was obtained in the attempted automated solid phase synthesis of a RboP-octa- and dodecamer.[10] As suggested by the authors, this could have been caused by the high concentration of TCA used to remove the DMTr groups. In our solution phase syntheses described above, we used a milder acid, DCA, for the removal of the DMTr

Chemistry–A European Journal

Full Paper
doi.org/10.1002/chem.202101242

Chemistry Europe
European Chemical
Societies Publishing

Scheme 3. Automated solid phase assembly of WTA-fragments. Reagents and conditions: a) 3% DCA in toluene (3 min); **12** or **15** BTT, ACN (5 min); I_2, pyr/H_2O (1 min); Ac_2O, N-methylimidazole, 2,6-lutidine, ACN (0.2 min); b) 25% NH_3 (aq) (60 min); **70**: 15%; **71**: 11%; **72**: 20%; **73**: 11%; c) Pd black, H_2, dioxane H_2O, AcOH, **2**: 100%; **3**: 100%; **10**: 87%; **11**: 100%.

group and these conditions were here translated to the solid phase. The syntheses were performed on an Äkta oligopilot plus™ synthesizer on 10 μmol scale (Scheme 2). The DMTr group was cleaved from resin **68** using 3% DCA in toluene and the coupling with cyanoethyl (CNE) amidite **12** under 5-(Benzylthio)-1H-tetrazole (BTT) activation then provided the resin bound phosphite. Oxidation using I_2 in pyridine/H_2O yielded the phosphate triester after which a capping step took place to prevent any unreacted alcohol functionalities to react in the next step, which could lead to byproducts that are difficult to separate. Removal of the DMTr group allowed a new cycle to start and the coupling cycles were repeated 7 and 11 times to reach the target octa- and dodecamer. Treatment of the resin with 3% DCA unmasked the primary alcohol and subsequent treatment with aqueous 25% NH_3 cleaved the cyanoethyl groups and released the oligomers from the resin. Scheme 3B depicts the LCMS chromatogram of the crude products **70** and **71**, indicating highly efficient syntheses of these oligomers. Purification of the crude oligomers by reversed phase HPLC and desalting afforded **70** and **71** in 15% and 11% yield respectively. Hydrogenation of the semi-protected octa- and dodecamer yielded the targets **2** and **3** both in quantitative yields. We also probed the use of GlcNAc carrying building blocks in the automated solid phase synthesis and assembled hexamers **10** and **11**, having either one or two β-(1,3)-GlcNAc appendages. Also these syntheses proceeded uneventfully, as judged from the amount of released DMT-groups and the benzyl protected target hexamers **72** and **73** were obtained in 20% and 11% yield, after reversed HPLC and a desalting step. Final hydrogenolysis of the semi-protected hexamers gave the target structures **10** and **11** in 87% and quantitative yield, respectively.

Characterization of glycosylated hexamers

We characterized the assembled oligomers by ^{1}H, ^{13}C and ^{31}P NMR and Figure 3 depicts the ^{1}H and ^{13}C spectra of the WTA

hexamers carrying two α-1-4-, β-1,4- or β-1,3-GlcNAc residues, namely compounds **5**, **8**, and **11**. The NMR spectra of these well-defined WTAs can be very useful for the structure determination of new WTA-species isolated from bacterial strains, in particular the position and configuration of these modifications along the chain. As shown in Figure 2A, the anomeric protons of the α-linked GlcNAc (in **5**) are present at a different chemical shift value than the anomeric protons of the β-GlcNAc (in **8** and **11**). The β-1,3-GlcNAc anomeric protons appear at 4.62 ppm, slightly lower than the β-1,4-GlcNAc anomeric protons with resonances at 4.70 ppm. These values are in accordance with those reported by Driguez and co-workers[4b] for β-1,3-GlcNAc modified WTA, isolated from strain ATC 55804 with an anomeric value of 4.65 and with β-1,4-GlcNAc WTA isolated from strain Wood 46 showing anomeric signals at 4.75 ppm. The reported anomeric signals for α-1,4-GlcNAc WTA from Newman D2C 5.07 (at 5.04 ppm) also agree well with the values for the α-1,4-GlcNAc WTA (5.03 ppm and 5.06 ppm). The values are also well in line with the TarP and TarM modified WTAs described by Gerlach et al.[8]

Figure 2B shows the ^{13}C NMR of the WTAs **5**, **8** and **11**. The anomeric signals of the β-1,3-GlcNAc WTA **11** appear at 101.6 and the C3 glycosylated Rbo **11** shows a shift for the ribitol C3 at 80.8 and 81.0 which is in agreement with the previously reported data, which described a chemical shift of 81.8 ppm for this carbon, appearing at a higher ppm value than the non-glycosylated ribitol positions.[8] The β-1,4-GlcNAc WTA **8** anomeric shifts can be found at 101.4 ppm and 101.6 ppm, comparable to the β-1,3-GlcNAc anomeric signals. The Rbo C4 of this β-1,4-glycosylated hexamer appear around 79.4-79.9, which is in accordance with the value previously reported (δ = 80.8 ppm) for glycosylated C-4 RboP-carbon atoms. The anomeric signals corresponding to the α-1-4-GlcNAc WTA **5** appear at 96.4 ppm and 96.5 ppm. This smaller chemical shift is expected for α-glycosidic linkages and the RboP C4 can be found at 77.6–77.8 ppm.

^{31}P NMR spectra have previously not been described for different glycosylated WTA oligomers. As depicted in Figure 2C,
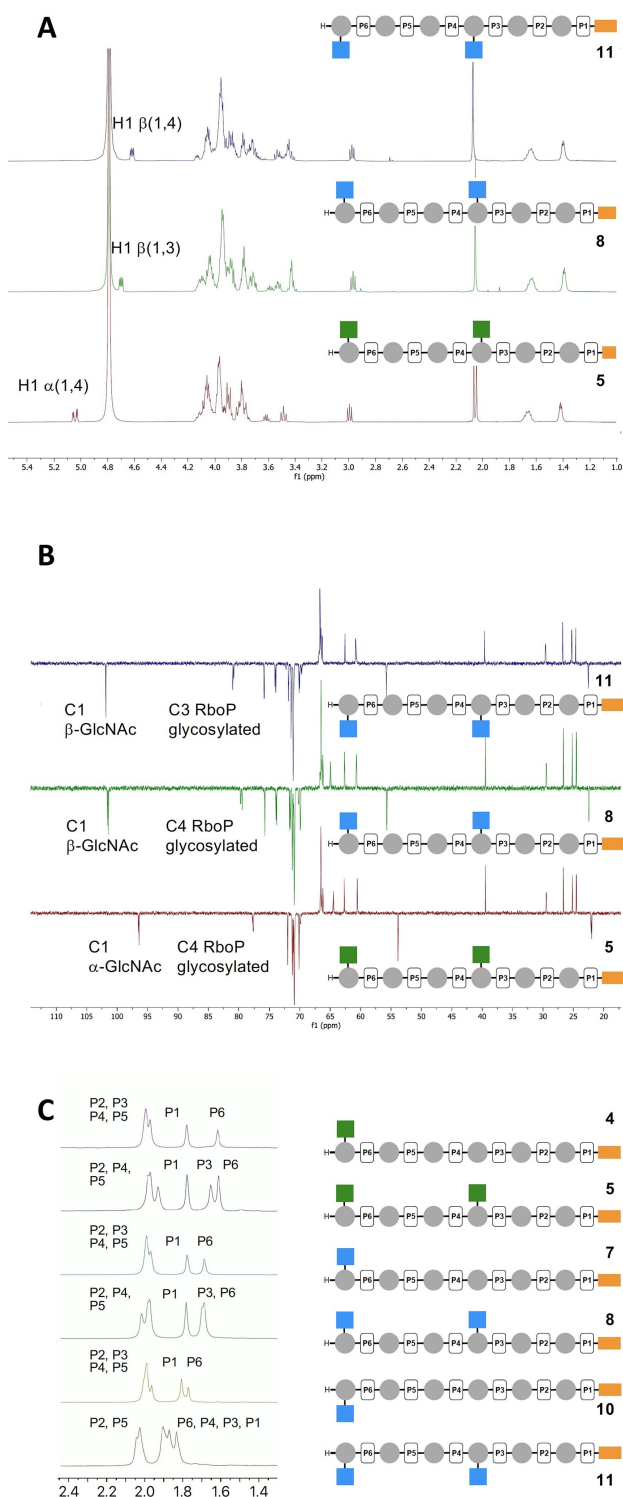
Chemistry–A European Journal

Full Paper
doi.org/10.1002/chem.202101242

Chemistry Europe
European Chemical
Societies Publishing

Figure 3. Characterization of the synthetic WTA-fragments. A) ^{1}H NMR (500 MHz, D$_2$O) of **5**, **8** and **11**. B) ^{13}C NMR (126 MHz, D$_2$O) of **5**, **8** and **11**. C) ^{31}P NMR (202 MHz, D$_2$O, 10 mg/mL, pH 7) of **4**, **5**, **7**, **8**, **10** and **11**.

the schematic structure diagrams next to the spectra. The spectrum of the αα-1,4-GlcNAc hexamer **5** shows three types of signals: three around 2 ppm, a single peak at 1.8 ppm and two peaks around 1.7 ppm. Considering that the phosphate next to the spacer will be different from the other phosphate diesters that are all flanked by two ribitol residues the single peak likely corresponds to the phosphate diester attached to the spacer. When the spectra of the α-1,4-GlcNAc- and αα-1,4-GlcNAc hexamers **4** and **5**, respectively, are compared it becomes clear that one peak has shifted to a lower ppm value. This phosphorous resonance thus likely corresponds to P$_3$. This analysis also holds for the β-1,4-GlcNAc- and ββ-1,4-GlcNAc hexamers **7** and **8**, which show a similar chemical shift pattern. The ^{31}P-spectrum of the β-1,3 glycosylated WTAs **10** and **11** shows similarity to the β-1,4- and α-1,4-GlcNAc WTAs. The introduction of the second GlcNAc substituent at the third ribitol residue causes the resonance of the phosphate diesters P$_3$ and P$_4$ (which are equally close to the GlcNAc residue in the middle of the RboP moiety) to shift to a lower chemical shift: the peaks around 1.8–1.9, corresponding to four P signals, belong to P$_1$, P$_3$, P$_4$ and P$_6$. The phosphodiesters, flanked by two non-substituted ribitols are found around 2 ppm. In all, this analysis shows that ^{31}P NMR chemical shifts can be diagnostic for the substitution pattern along the RboP chain, and the relative intensity of the signals indicative for the degree of glycosylation.

Antibody binding

With the synthetic WTA fragments in hand, we set out to develop an assay to interrogate antibody binding. Recently, Lupardus and co-workers have described the development of different monoclonal antibodies, generated from B-cells of *S. aureus* infected patients.[18] Structural studies were performed with these mAbs using X-ray crystallography on a monomeric β-1,4-GlcNAc ribitol phosphate fragment and binding studies were performed with whole bacteria, using biosynthesis knock-out strains to unravel the role of the WTA-glycosylation pattern.[19] The availability of our synthetic fragments now allows for direct binding studies at the molecular level. We have recently described the development of a magnetic bead assay to study the deposition of antibodies through binding of enzymatically glycosylated WTA fragments.[12] We here used the same set up and equipped the synthesized hexamers with a biotin handle, exploiting the amine function of the hereto introduced amino spacer (Figure 4A). Next, streptavidin-coated magnetic dynabeads M280 were functionalized with the biotinylated hexamers and then interrogated using monoclonal antibodies, generated to recognize α-GlcNAc functionalized RboP WTAs (clone 4461 and clone 4624) or β-1,4-GlcNAc carrying RboP WTAs (clones 4497 and 6292).

As can be seen in Figure 4B, mAb 4461 binds to the beads functionalized with the WTA fragments carrying an α-GlcNAc appendage **4** and **5**. The non-glycosylated RboP-hexamers or the hexamers carrying β-GlcNAc-residues are not recognized by this antibody. A single α-GlcNAc-functionality (as in **4**) seems to
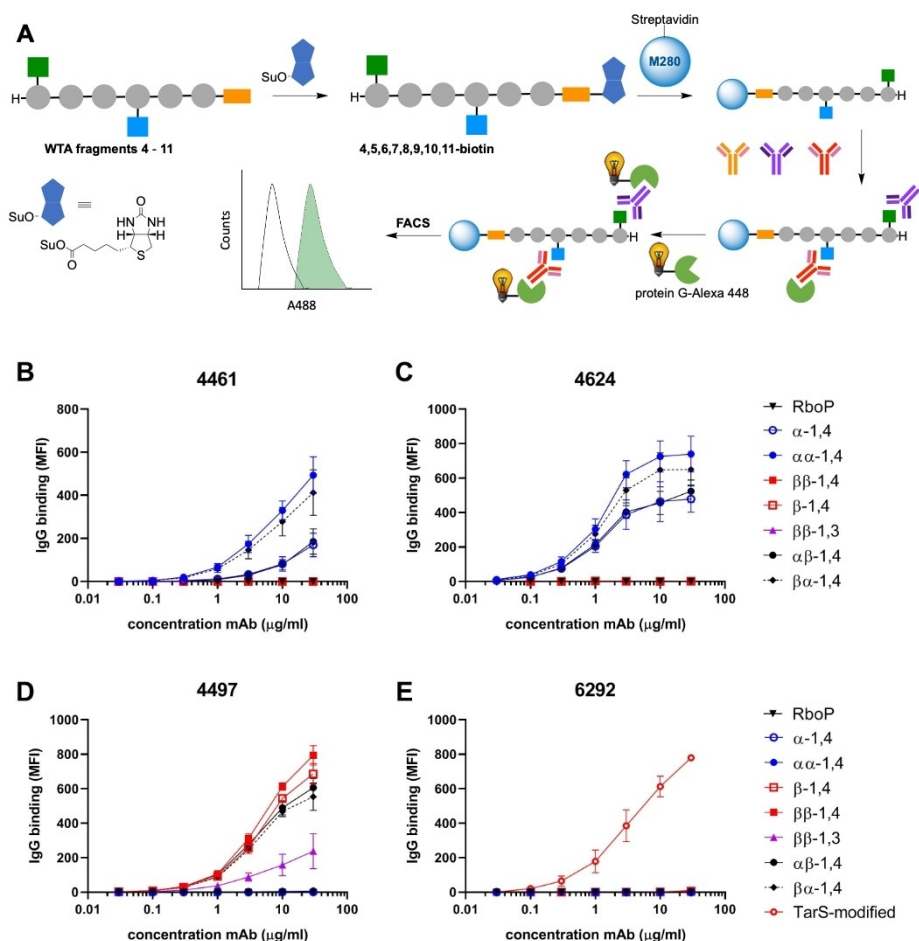
comparing the ^{31}P NMR spectra of the α-1,4-GlcNAc WTA, β-1,4-GlcNAc WTA and β-1,3-GlcNAc WTA hexamers, it appears that the ^{31}P-chemical shift is diagnostic for the type of GlcNAc appendage. The ^{31}P signals are assigned P$_1$ to P$_6$, as shown in

Chemistry–A European Journal

Full Paper
doi.org/10.1002/chem.202101242

Chemistry Europe
European Chemical
Societies Publishing

Figure 4. Magnetic WTA-beads for antibody binding assays. A) Workflow for the antibody binding assay: 1) Biotinylation of WTA fragments **4–11**; 2) Adsorption on streptavidin coated M280 Dynabeads; 3) binding of monoclonal antibodies; 4) Alexa 488-Protein G conjugation; 5) Readout of fluorescent beads. B–E) Binding of monoclonal antibody B) 4461, C) 4624, D) 4497 and E) 6292 to the WTA-functionalized beads.

be sufficient for binding, but the beads functionalized with two α-GlcNAc-residues (as in **5**) show increased binding. The presence of a β-1,4-GlcNAc in the WTA fragments does not interfere with binding as the αβ-1,4 (**9**) and βα-1,4 (**6**) functionalized beads both show deposition of the antibody. Interestingly the αβ-1,4-GlcNAc **9** functionalized beads show less antibody binding than the corresponding βα-1,4 (**6**) derivatized beads. This may indicate that the mAb binds better to "internal" α-GlcNAc-residues than to an α-GlcNAc at the terminus of the WTA chain. The analysis of clone 4624 provides a nearly identical picture: α-GlcNAc-functionalized WTA fragments are selectively recognized with a single sugar residue being the minimal requirement for binding (Figure 4C). Also this mAb seems to have a preference for internal α-GlcNAc-residues.

Clones 4497 and 6292 have been identified to recognize β-1,4-GlcNAc-WTA and Figure 4D shows that 4497 binds to all WTA-hexamers carrying a β-1,4-GlcNAc-residue. A single β-1,4-GlcNAc-moiety seems to be sufficient for binding and there does not seem to be a strong preference for the position of the β-1,4-GlcNAc on the WTA chain. This mAb also binds to the

regioisomeric β-1,3-GlcNAc epitopes (**11**), indicating that this mAb is cross-reactive to TarP-expressing *S. aureus*. The binding to the β-1,3-GlcNAc-WTA fragment **11** is however, significantly weaker than binding to its β-1,4-counterpart **8**. The binding assays using clone 6292 (Figure 4E) show that the synthetic fragments are poorly recognized by this mAb. In contrast, the hexamers glycosylated using the β-1,4-GlcNAc-transferase TarS do induce antibody deposition on the beads. The hexamers that have been enzymatically glycosylated have a higher density of β-1,4-GlcNAc-residues (an average of 3–4 GlcNAc residues per hexamer) indicating that this mAb either binds preferentially to WTA fragments carrying multiple β-1,4-GlcNAc-residues in close proximity or that the affinity of this mAb is lower and thus requires the simultaneous presentation of multiple epitopes, within the same WTA-fragment.

Conclusion

We describe here a synthetic chemistry approach to assemble all currently known glycosylation types of *S. aureus* RboP WTAs.

Chemistry–A European Journal

Full Paper
doi.org/10.1002/chem.202101242

**Chemistry
Europe**
European Chemical
Societies Publishing

We have developed stereoselective glycosylation reactions to generate building blocks that have been used to assemble α-1,4, β-1,4 and β-1,3-GlcNAc functionalized RboP-WTAs. A strategy was used employing phosphoramidite chemistry in combination with DMTr-protected building blocks. This "DNA-type" chemistry was successfully transposed to an automated solid phase format, significantly streamlining the assembly of longer WTA fragments. Detailed spectroscopic analysis of the fragments has revealed diagnostic signals that can be used as reference for future WTA-structure elucidation studies. Finally, we have shown the applicability of the synthetic WTA-fragments in the development of a binding assay to map binding interactions of anti-WTA monoclonal antibodies at the molecular level. These interaction studies have shown that antibodies that recognize β-1,4-GlcNAc WTA can be cross-reactive with β-1,3-GlcNAc WTA. It is thus likely that IgG in human serum is also capable of interacting with both TarS-WTA and TarP-WTA, as described by Van Dalen et al.[12] More detailed binding studies are required to pinpoint the differences in binding between the two different epitopes and the (recombinantly expressed) monoclonal antibodies or human sera. It is expected that raising antibodies against *S. aureus* TarP-WTA, or a synthetic conjugate featuring this WTA-type will lead to specific anti-β-1,3-GlcNAc-WTA antibodies. Alternatively, structure-guided antibody engineering may open up avenues to generate selective and tight binding WTA-glycosylation type specific antibodies. Well-defined WTA fragments are valuable tools to delineate clear structure-activity relationships and will be used in the future to characterize antibody binding epitopes and to probe binding to other receptors, such as C-type lectins and unravel the mode of action of biosynthesis enzymes at the molecular level.

Acknowledgements

Conflict of Interest

The authors declare no conflict of interest.

[1] F. D. Lowy, *N. Engl. J. Med.* **1998**, *339*, 520.

[2] C. P. Harkins, B. Pichon, M. Doumith, J. Parkhill, H. Westh, A. Tomasz, H. De Lencastre, S. D. Bentley, A. M. Kearns, M. T. G. Holden, *Genome Biol.* **2017**, *18*, 130.

[3] R. S. Daum, B. Spellberg, *Clin. Infect. Dis.* **2012**, *54*, 560.

[4] a) A. Fattom, (Nabi Biopharmaceuticals), WO 2007/053176 A2, **2007**; b) P.-A. G. Driguez, (Sanofi Pasteur), WO 2017/064190 A1, **2017**; c) R. Adamo, A. Nilo, B. Castagner, O. Boutureira, F. Berti, G. J. Bernardes, *Chem. Sci.* **2013**, *4*, 2995.

[5] F. C. Neuhaus, J. Baddiley, *Microbiol. Mol. Biol. Rev.* **2003**, *67*, 686.

[6] S. Sobhanifar, L. J. Worrall, D. T. King, G. A. Wasney, L. Baumann, R. T. Gale, M. Nosella, E. D. Brown, S. G. Withers, N. C. Strynadka, *PLoS Pathog.* **2016**, *12*, e1006067.

[7] S. Sobhanifar, L. J. Worrall, R. J. Gruninger, G. A. Wasney, M. Blaukopf, L. Baumann, E. Lameignere, M. Solomonson, E. D. Brown, S. G. Withers, N. C. Strynadka, *Proc. Natl. Acad. Sci. USA* **2015**, *112*, E576.

[8] D. Gerlach, Y. Guo, C. De Castro, S. H. Kim, K. Schlatterer, F. F. Xu, C. Pereira, P. H. Seeberger, S. Ali, J. Codee, W. Sirisarn, B. Schulte, C. Wolz, J. Larsen, A. Molinaro, B. L. Lee, G. Xia, T. Stehle, A. Peschel, *Nature* **2018**, *563*, 705.

[9] a) W. F. Hogendorf, L. J. Bos, H. S. Overkleeft, J. D. Codee, G. A. Marel, *Bioorg. Med. Chem.* **2010**, *18*, 3668; b) D. van der Es, W. F. Hogendorf, H. S. Overkleeft, G. A. van der Marel, J. D. Codee, *Chem. Soc. Rev.* **2017**, *46*, 1464; c) D. van der Es, F. Berni, W. F. J. Hogendorf, N. Meeuwenoord, D. Laverde, A. van Diepen, H. S. Overkleeft, D. V. Filippov, C. H. Hokke, J. Huebner, G. A. van der Marel, J. D. C. Codee, *Chem. Eur. J.* **2018**, *24*, 4014; d) W. F. Hogendorf, L. N. Lameijer, T. J. Beenakker, H. S. Overkleeft, D. V. Filippov, J. D. Codee, G. A. Van der Marel, *Org. Lett.* **2012**, *14*, 848; e) W. F. Hogendorf, A. Kropec, D. V. Filippov, H. S. Overkleeft, J. Huebner, G. A. van der Marel, J. D. Codee, *Carbohydr. Res.* **2012**, *356*, 142.

[10] A. Fekete, P. Hoogerhout, G. Zomer, J. Kubler-Kielb, R. Schneerson, J. B. Robbins, V. Pozsgay, *Carbohydr. Res.* **2006**, *341*, 2037.

[11] Y. C. Jung, J. H. Lee, S. A. Kim, T. Schmidt, W. Lee, B. L. Lee, H. S. Lee, *Org. Lett.* **2018**, *20*, 4449.

[12] R. van Dalen, M. M. Molendijk, S. Ali, K. P. M. van Kessel, P. Aerts, J. A. G. van Strijp, C. J. C. de Haas, J. Codée, N. M. van Sorge, *Nature* **2019**, *572*, E1.

[13] D. Laverde, D. Wobser, F. Romero-Saavedra, W. Hogendorf, G. van der Marel, M. Berthold, A. Kropec, J. Codee, J. Huebner, *PLoS One* **2014**, *9*, e110953.

[14] J. P. G. Hermans, L. Poot, M. Kloosterman, G. A. van der Marel, C. A. A. van Boeckel, D. Evenberg, J. T. Poolman, P. Hoogerhout, J. H. van Boom, *Recl. Trav. Chim. Pays-Bas* **1987**, *106*, 498.

[15] I. Figueroa-Perez, A. Stadelmaier, S. Morath, T. Hartung, K. R. Schmidt, *Tetrahedron: Asymmetry* **2005**, *16*, 493.

[16] a) T. Tsuda, S. Nakamura, S. Hashimoto, *Tetrahedron* **2004**, *60*, 10711; b) J.-R. Pougny, P. Sinaÿ, *Tetrahedron Lett.* **1976**, *17*, 4073; c) R. R. Schmidt, M. Behrendt, A. Toepfer, *Synlett* **1990**, *11*, 694; d) R. R. Schmidt, E. Rücker, *Tetrahedron Lett.* **1980**, *21*, 1421; e) S. K. Mulani, W. C. Hung, A. B. Ingle, K. S. Shiau, K. K. Mong, *Org. Biomol. Chem.* **2014**, *12*, 1184; f) E. A. Khatuntseva, A. A. Sherman, Y. E. Tsvetkov, N. E. Nifantiev, *Tetrahedron Lett.* **2016**, *57*, 708; g) A. V. Demchenko, *Handbook of Chemical Glycosylation;* A. V. Demchenko, Ed., Wiley-VCH Verlag GmbH & Co. KGaA: Weinheim, Germany, **2008**, pp. 10–11; h) D. van der Es, N. A. Groenia, D. Laverde, H. S. Overkleeft, J. Huebner, G. A. van der Marel, J. D. Codee, *Bioorg. Med. Chem.* **2016**, *24*, 3893.

[17] W. Sowa, G. H. S. Thomas, *Can. J. Chem.* **1966**, *44*, 836.

[18] R. Fong, K. Kajihara, M. Chen, I. Hotzel, S. Mariathasan, W. L. W. Hazenbos, P. J. Lupardus, *mAbs* **2018**, *10*, 979.

[19] J.-H. Lee, N.-H. Kim, V. Winstel, K. Kurokawa, J. Larsen, J.-H. An, A. Khan, M.-Y. Seong, M. J. Lee, P. S. Andersen, A. Peschel, B.-L. Lee, *Infect. Immun.* **2015**, *83*, 4247.